



Geophysical Research Letters

RESEARCH LETTER

10.1002/2017GL075226

Key Points:

- Multiobjective optimization applied to multiple observational climate model constraints helps generalize emergent constraint approaches
- Subensembles interpolate model spatial fields and aid evolutionary algorithm estimation of a robust Pareto front for historical constraints
- Model subensembles that are Pareto-optimal by observational criteria are used to constrain projections of future California precipitation

Supporting Information:

- Supporting Information S1

Correspondence to:

B. Langenbrunner,
blangenb@uci.edu

Citation:

Langenbrunner, B., &
Neelin, J. D. (2017). Pareto-optimal
estimates of California precip-
itation change. *Geophysical
Research Letters*, 44, 12,436–12,446.
<https://doi.org/10.1002/2017GL075226>

Received 10 AUG 2017

Accepted 12 SEP 2017

Accepted article online 18 SEP 2017

Published online 18 DEC 2017

Pareto-Optimal Estimates of California Precipitation Change

Baird Langenbrunner^{1,2}  and J. David Neelin¹ 

¹Department of Atmospheric and Oceanic Sciences, University of California, Los Angeles, CA, USA, ²Department of Earth System Science, University of California, Irvine, CA, USA

Abstract In seeking constraints on global climate model projections under global warming, one commonly finds that different subsets of models perform well under different objective functions, and these trade-offs are difficult to weigh. Here a multiobjective approach is applied to a large set of subensembles generated from the Climate Model Intercomparison Project phase 5 ensemble. We use observations and reanalyses to constrain tropical Pacific sea surface temperatures, upper level zonal winds in the midlatitude Pacific, and California precipitation. An evolutionary algorithm identifies the set of Pareto-optimal subensembles across these three measures, and these subensembles are used to constrain end-of-century California wet season precipitation change. This methodology narrows the range of projections throughout California, increasing confidence in estimates of positive mean precipitation change. Finally, we show how this technique complements and generalizes emergent constraint approaches for restricting uncertainty in end-of-century projections within multimodel ensembles using multiple criteria for observational constraints.

1. Introduction

Accurate projections of precipitation change along the North American west coast are crucial to long-term water resource planning, and narrowing the spread in these changes among global climate models has been a consistent and significant challenge. California in particular lies in a transition zone between robust increases to the north and decreases to the south, and in central and southern parts of the state, the ability to draw conclusions on mean wet season precipitation change has been hindered by large intermodel disagreement in the Climate Model Intercomparison Project phase 5 (CMIP5) archive (Collins et al., 2013; Flato et al., 2013; Neelin et al., 2013; Seager et al., 2014).

Mechanisms for hydrological cycle change are reasonably well understood at large spatial scales, though this breaks down at the regional level. Thermodynamic arguments predict that at large scales and over the ocean, regions of climatological moisture convergence tend to get wetter (the tropics and middle to high latitudes) and regions of climatological moisture divergence tend to get drier (the subtropics) (Chou & Neelin, 2004; Held & Soden, 2006; Trenberth, 2011). On smaller spatial scales and over land, however, dynamical factors also become important (e.g., Greve et al., 2014; Roderick et al., 2014), including changes in the Hadley cell (Lu et al., 2007; Scheff & Frierson, 2012a, 2012b; Su et al., 2014) and meridional shifts of the midlatitude Pacific storm track (Chang et al., 2012). CMIP5 models exhibit notable disagreement in these dynamical responses to warming. For California specifically, intermodel spread in precipitation change has been attributed to uncertainty in jet stream position/variability, stationary wave patterns, and coupled ocean-atmosphere dynamics originating in the tropical Pacific (Allen & Luptowitz, 2017; Chang et al., 2015; Choi et al., 2016; Delambre et al., 2013a, 2013b; Langenbrunner et al., 2015; Neelin et al., 2013; Seager et al., 2014; Simpson et al., 2016).

When attempting to constrain regional climate change uncertainty within an “ensemble of opportunity” like CMIP5, researchers often create metrics of model performance to narrow the range of projections. A single best model or model subset is difficult to select across multiple measures (Gleckler et al., 2008; Pierce et al., 2009, 2013; Pincus et al., 2008; Reichler & Kim, 2008; Santer et al., 2009), as improvement in one metric is often accompanied by degradation in another, and these trade-offs can be difficult to reconcile. And although the ensemble mean commonly outperforms individual members, the prevailing one-model-one-vote approach has been criticized (Knutti, 2010; Knutti et al., 2010; Sanderson & Knutti, 2012; Tebaldi & Knutti, 2007), in part because models share components and are not independent (Knutti et al., 2013; Masson & Knutti, 2011).

In response, techniques have been developed to analyze an ensemble more thoughtfully—for example, tools that weight models by skill and independence (Abramowitz & Bishop, 2015; Bishop & Abramowitz, 2013; Herger et al., 2017; Knutti et al., 2017; Sanderson et al., 2017) or using Bayesian techniques (e.g., Tebaldi & Sansó, 2009).

An alternative approach comes from the emergent constraint literature, where researchers seek a metric in the current climate that correlates well among models with end-of-century projections and then use observations to place constraints on this measure. This technique was introduced by Hall and Qu (2006) in the context of snow albedo feedback, and it has since been applied widely, with the majority of studies examining equilibrium climate sensitivity and moisture and cloud feedbacks (Brient et al., 2016; Ceppli et al., 2016; DeAngelis et al., 2015; Fasullo & Trenberth, 2012; Gordon & Klein, 2014; Klocke et al., 2011; Myers & Norris, 2016; Qu et al., 2015; Sherwood et al., 2014; Su et al., 2014, 2017; Tian, 2015; Trenberth and Fasullo, 2010; Tsushima et al., 2016; Volodin, 2008; Zhai et al., 2015). This approach was also used in the latest Intergovernmental Panel on Climate Change (IPCC) Fifth Assessment Report (AR5, Stocker et al., 2013), where Arctic sea ice projections were constrained using models that perform well in recent historical climate (see Collins et al., 2013, chap. 12 and Figure 12.31). While useful in certain applications, these methods depend on the existence of a single, high-correlation predictor between historical and future climates with physically credible mechanisms (Klein & Hall, 2015), and these are hard to find for certain aspects of uncertainty in the climate system—for example, the California precipitation change problem, for which emergent constraint approaches have arrived at opposing conclusions (Allen & Luptowitz, 2017; Simpson et al., 2016). Because of this, a more flexible technique that generalizes these approaches and handles multiple constraints is needed.

This study uses multiobjective optimization techniques to identify model subsets that perform more accurately than individual models or the ensemble mean across multiple historical climate metrics simultaneously. These techniques are designed to quantify performance trade-offs in a wide variety of systems (e.g., Branke et al., 2008; Coello Coello et al., 2007; Marler & Arora, 2004) and have been used in climate model applications (Langenbrunner & Neelin, 2017; Neelin et al., 2010). The concept we focus on is that of Pareto optimality, where improvement in one measure of performance cannot occur without degradation in another. A multi-objective approach finds Pareto-optimal model fields based on comparison to observations, and these form a surface called a Pareto front that is used to constrain end-of-century projections. An ensemble with a size typical of CMIP5 (tens of members) does not span objective function space smoothly enough for these techniques to be applied directly, so we use subsets of models, or subensembles, to interpolate more continuously in the simulated climate field space. We apply this approach to three fields in the historical climatology that we hypothesize are relevant to California precipitation and uncertainty in its projections: tropical Pacific sea surface temperatures (SSTs), 200 hPa zonal wind, and California precipitation. These Pareto-optimal techniques offer an alternative methodology for placing observational constraints on climate model ensemble projections. We also present an example that clarifies the relationship between our approach and that of the emergent constraint literature.

2. Model Data and Observational Constraints

Single climate model realizations for precipitation, ocean skin temperature, and 200 hPa zonal wind fields are used for 36 models in the CMIP5 archive (Taylor et al., 2012) and 40 ensemble members from the National Center for Atmospheric Research Large Ensemble (NCAR LENS) archive (Kay et al., 2015). End-of-century changes discussed below represent the difference between 30 year December–January–February (DJF) climatologies for historical (1980–2010) and Representative Concentration Pathway 8.5 (RCP8.5, 2070–2100) forcing scenarios.

Observational and reanalysis data sets include precipitation from the Global Precipitation Climatology Project (GPCP) (Adler et al., 2003), skin temperature from the ERA-Interim reanalysis (Dee et al., 2011), and 200 hPa zonal winds from the Modern Era Retrospective Reanalysis (MERRA) (Rienecker et al., 2011). Skin temperature is taken over ocean-only grid points and is equivalent to SST fields. All modeled/reanalyzed data were regridded to a $2.5^\circ \times 2.5^\circ$ resolution via linear interpolation prior to analysis, and 1980–2010 was analyzed for all data sets.

Figures 1a–1c show the CMIP5 climatologies and biases for these fields. For precipitation (Figure 1a), the CMIP5 ensemble mean shows a positive bias in orographic coastal regions along the California coast, with a negative bias as the coast extends north toward Canada and Alaska. For SSTs, the ensemble mean is biased

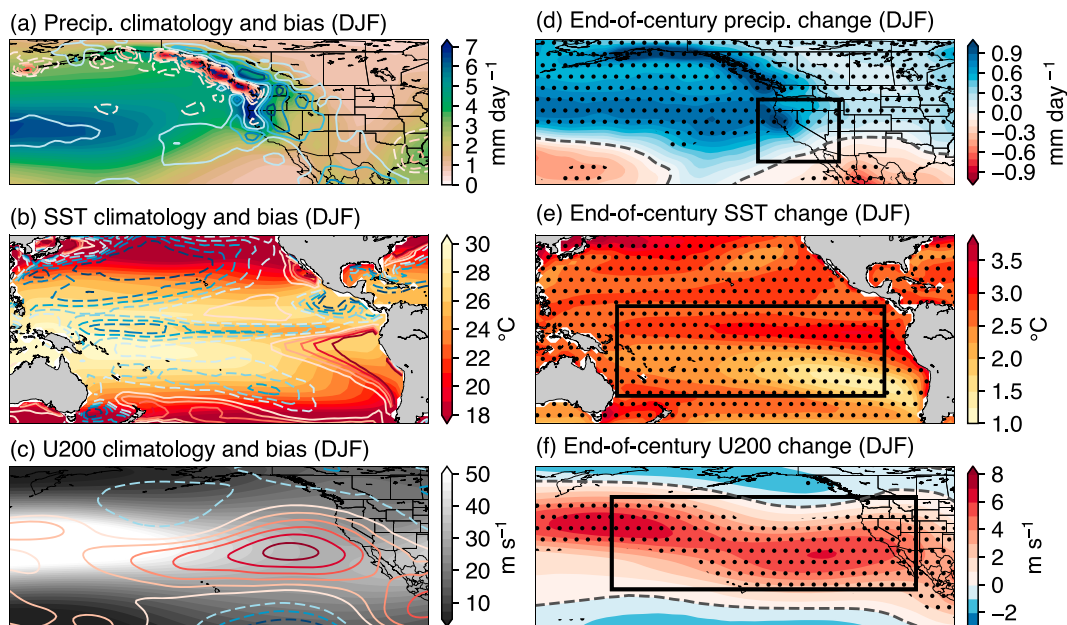


Figure 1. Ensemble mean climatological fields, historical biases, and end-of-century changes during DJF for 36 models in the CMIP5 archive (see Figure 2 for models). CMIP5 ensemble mean climatological fields shown as filled contours for (a) precipitation, (b) SSTs, and (c) 200 hPa zonal winds, as well as CMIP5 ensemble mean minus-observed biases as contour lines (negative values are dashed and the zero line is omitted); intervals in each panel are 0.5 mm d^{-1} (Figure 1a), 0.25°C (Figure 1b), and 1 m s^{-1} (Figure 1c). CMIP5 ensemble mean end-of-century changes are shown in Figures 1d-f. Objective function calculations discussed in this manuscript are performed over regions outlined in black boxes; the corner latitudes/longitudes of these are (d) 30°N – 45°N / 232.5°E – 248°E , (e) 30°S – 10°N / 155°E – 270°E , and (f) 20°N – 50°N / 170°E – 250°E . Maps in Figures 1d–1f are stippled where more than 80% of models agree on sign of change.

cold in DJF throughout much of the tropical Pacific (Figure 1b), with notable signals in the tropical western Pacific and central midlatitude northern Pacific, and it also exhibits maximum warm biases near shallow cumulus regions and in the midlatitude southern Pacific. The ensemble mean bias in 200 hPa wind is positive throughout the eddy-driven jet region to the east of the jet maximum (Figure 1c), indicating a jet that is too fast over the eastern Pacific.

Figures 1d–1f show end-of-century CMIP5 ensemble mean changes. The precipitation change dipole along the North American west coast (Figure 1d), with increases to the north and decreases to the south, portrays the intermodel disagreement discussed in the introduction (see Figure S1 in the supporting information for individual model precipitation change plots). SSTs increase everywhere (Figure 1e), with largest tropical changes along the equatorial Pacific in the cold tongue region. The 200 hPa winds show a slight northward shift in the western Pacific and an in-place increase and eastward extension of the jet in the eastern Pacific (Figure 1f), where the maximum changes are approximately collocated with the largest positive biases in Figure 1c.

The domains outlined in black in Figures 1d–1f show the regions over which the objective functions are calculated below. These are chosen for their physical relevance to the California hydrological cycle: a precipitation domain encompassing California, a large tropical Pacific SST region, and 200 hPa zonal winds in a box approaching the North American west coast. The SST and wind fields are chosen to serve as proxies for important mean state processes affecting the California hydrological cycle. The tropical Pacific SST domain represents the source region of tropical-to-midlatitude teleconnections associated with model spread in California precipitation change (Allen & Luptowitz, 2017; Langenbrunner et al., 2015). Upper level zonal winds are used as a measure of two physical mechanisms. First, the upper level flow exerts a leading control on the dynamics of planetary waves, and Simpson et al. (2016) found that uncertainty in wave propagation in this region is a primary source of CMIP5 model spread for California hydrological cycle change. Second, the midlatitude jet steers storms toward the California coast, and model biases in its position are associated with intermodel uncertainty in precipitation projections (Chang et al., 2015; Langenbrunner et al., 2015).

Neelin et al., 2013). Finally, we include precipitation to ensure that our multiobjective criteria take into account climate model performance in this field. While this third metric is not associated with an emergent constraint, it serves the purpose of excluding from the Pareto front model subsets that do poorly at simulating California precipitation.

3. Pareto-Optimal Subensembles for Historical Climatologies

3.1. Generating Subensembles

When models are weighted equally, the number of unique k -member subensembles that can be generated from an N -model ensemble is $\binom{N}{k}$ or “ N choose k .” We view subensemble averages as interpolations in climatological field space (see Figure S2), and so in calculations here, we include all subensembles created for model subsets of size $\leq k$, giving $\sum_{i=1}^k \binom{N}{i}$ members. Here $N = 36$ and $k \in [1, 5]$, so $\sum_{i=1}^5 \binom{36}{i} = 443,703$. For each of these, subensemble means are generated for precipitation, SST, and 200 hPa wind climatologies during the historical period, and the spatial root-mean-square error (RMSE) of each field is calculated for the domains in Figure 1. These RMSE values are shown as gray clouds of points in two- and three-dimensional objective function space in Figures 2a–2d, in which the origins represent a model/subensemble performing perfectly (assuming accurate observations or reanalyses). Individual CMIP5 simulations are included as colored rings and represent $k = 1$, and the CMIP5 ensemble mean is shown as an unfilled black square. Note that subensemble averages are taken on the spatial fields before the RMSE is calculated, and so the gray points do not represent averages of separate RMSE values. Because of this, the RMSE values of subensembles can be less than that of any individual model.

A parallel set of steps was taken for the 40 NCAR LENS simulations, for which $\sum_{i=1}^5 \binom{40}{i} = 760,098$. Small black points in Figures 2a–2c represent original NCAR LENS runs, and the underlying orange points show subensembles. The spread of the orange points in objective function space serves as a measure of sampling error or internal variability generated within one climate model; that these black and orange points are grouped tightly relative to individual CMIP5 models or the gray cloud of points implies that the variation among CMIP5 models here is not a result of internal variability, but rather genuine intermodel differences (see also Figure S3 and the related discussion in the supporting information).

To visualize observational and reanalysis error, a measure of sampling error due to internal variability is included as a yellow ellipse at the origin of each Pareto front in Figures 2a–2c. Note that the areal extent of this region is much smaller in comparison to the spread of individual CMIP5 models, implying that internal variability in these observational products will not have a leading-order affect on Pareto-optimal statistics.

We have explored the effect of different numbers of model combinations $k \in [1, 7]$ and have found that $k = 5$ is sufficiently large to achieve the full benefits of this approach while still keeping the number of computations reasonable (see Figures S3 and S4). We also refer the reader to Herger et al. (2017), who have conducted a comprehensive analysis on model subensembles while considering important aspects of model performance, independence, and spread.

3.2. Identifying Pareto-Optimal Subensembles for Historical Climatologies

Pareto optimality was originally discussed by Pareto (1906) in the context of allocating societal resources in a way that would leave no individual worse off, and it has since found wide application wherever design choices must be weighed across multiple objectives. An example is performance versus affordability in car design. Multiobjective optimization gives a precise way to eliminate car designs that do poorly in both measures, and it can identify the set of solutions that represent optimal trade-offs between affordability and performance. Choices could then be made from this Pareto-optimal set—for example, a manufacturer may offer a range of models from high-performance to budget conscious. This differs from conventional optimization procedures that use a weighted sum of objective functions, which for this example would result in a single, midrange option. In our application, objective functions represent the quality of climate model simulation in the historical climatology, and it is not always clear how to assign importance or weights to them. The Pareto front can therefore be thought of as the range of solutions associated with different weightings across metrics of interest. It also helps visualize the severity of these trade-offs: a “shorter” Pareto front (small extent in objective function space) implies that constraints are in accord, whereas a “longer” front indicates a broader set of trade-offs that require careful examination.

A large body of literature exists for identifying Pareto-optimal solutions in a given objective function space (e.g., Branke et al., 2008). To identify the Pareto fronts in Figure 2, we use the Nondominated Sorting Genetic

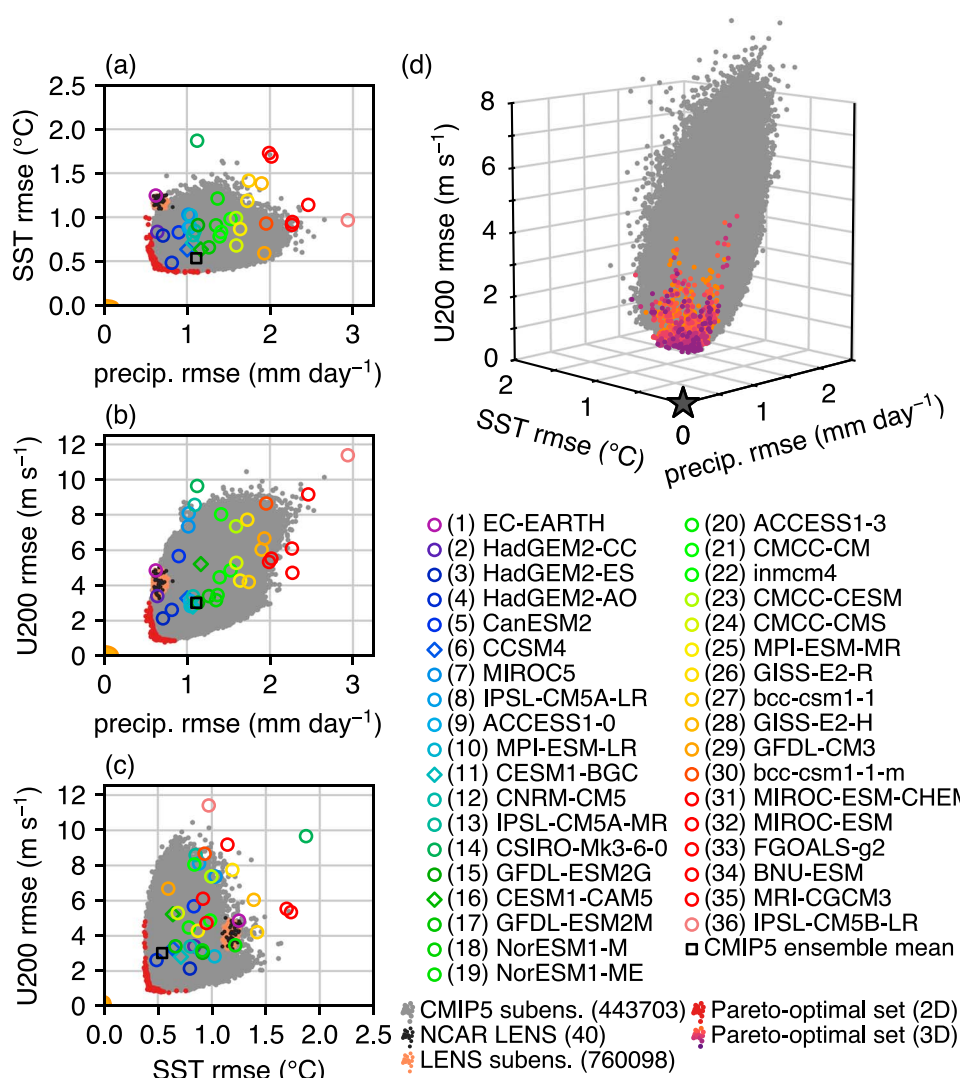


Figure 2. Performance of CMIP5 models, NCAR LENS simulations, and subensembles calculated for precipitation, 200 hPa zonal wind, and SST RMSE in the historical climatology. Objective functions are calculated over the areas outlined in Figure 1. (a–c) Two-dimensional Pareto fronts are shown as red dots. Colored rings represent individual CMIP5 models, and the gray clouds of points represent the 443,703 subensembles generated from CMIP5. Small black points represent 40 NCAR LENS simulations, and the underlying light orange cloud represents the 760,098 subensembles generated from these runs. Yellow ellipses at each origin in Figures 2a–2c represent the 95% confidence range of the internal variability in the observations/reanalyses. The vertical and horizontal radii of these represent $1.96 \times SE$, where $SE = \sigma / \sqrt{y}$ is the standard error of the mean RMSE value, σ is the standard deviation across yearly DJF RMSE values during the 1980–2010 record, and y is the number of years (here, 30). (d) Three-dimensional Pareto front, with dark gray star showing the origin (where a model or subensemble would be performing perfectly). Pareto fronts represent five successive passes of the evolutionary algorithm. Differently colored points in Figure 2d indicate these five iterations to convey dimensionality; purple indicates the first iteration and lightest orange the fifth.

Algorithm II (NGSA-II) developed by Deb et al. (2002) and implemented by Woodruff and Herman (2014). NGSA-II fits into the broader field of evolutionary algorithms (Coello Coello et al., 2007) and has been used to calibrate the deep convection scheme of a climate model in Langenbrunner & Neelin (2017). We make multiple passes of the algorithm to approximate a smooth front, and the depth or thickness is chosen to approximate the interpoint spacing typical in the set of subensembles. As the number of objective functions increases, successive iterations of the evolutionary algorithm help approximate a smooth surface with a large but finite number of points.

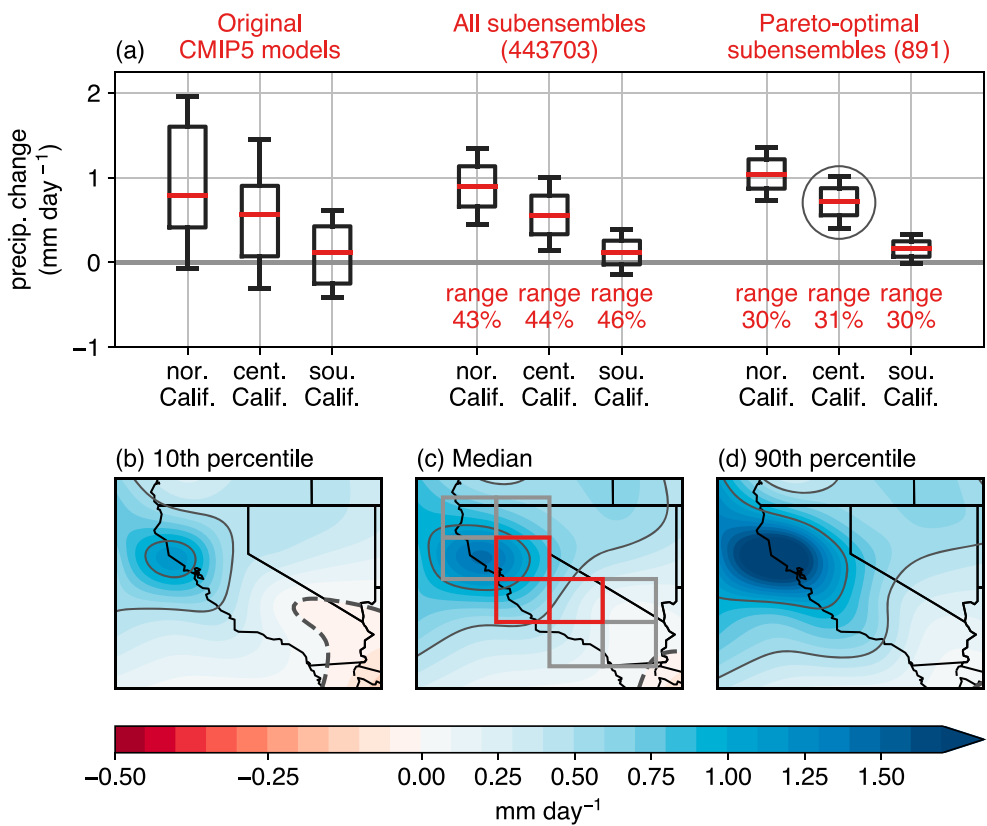


Figure 3. (a) Box and whisker plots showing the range of end-of-century projections for the full CMIP5 archive, for triplets of northern, central, and southern California grid boxes shown in Figure 3c). Boxes represent upper and lower quartiles (25th and 75th percentile) and the median (50th percentile; red line), and whiskers span the 10th to 90th percentiles of the full distributions. The left three distributions depict the original CMIP5 models, the middle three show changes for all CMIP5 subensembles (gray points in Figure 2d), and the right three show the Pareto-optimal solutions (Pareto front in Figure 2d). Percent values indicate the whisker range of each distribution as a fraction of the full CMIP5 whisker range. (b–d) Maps of precipitation change corresponding to three subensembles from the central California Pareto-optimal set (circled diagram in Figure 3a). Red squares in Figure 3b show the central California grid boxes, and gray squares show the northern and southern California grid boxes.

Pareto-optimal members for the CMIP5 subensembles are plotted as red points in Figures 2a–2c for solutions computed in two-dimensional objective function space. In these planes, the CMIP5 ensemble mean performs better than individual CMIP5 models, but it is still outperformed by members of the Pareto front. Figure 2d shows Pareto-optimal solutions calculated in three dimensions. The Pareto front can in principle be calculated across any number of dimensions, and it can change as objective functions are added to or removed from consideration. Here it is well behaved and consistent across Figures 2a–2d, and the fact that it occurs in a reasonably restricted region indicates that some subensembles are performing well by these measures. Colors in Figure 2d illustrate sequential iterations filling out the Pareto-optimal set, likewise indicating smooth behavior.

We note that our aim is not to find a single optimal model or subset but rather to identify the Pareto-optimal population of subensembles that can be used to generate useful statistics of ensemble performance. In the next section, we use this information to place constraints on California precipitation change.

4. Pareto-Optimal Subensemble Projections for California Precipitation Change

4.1. Uncertainty Range for Central California

We define precipitation change indices for northern, central, and southern California, calculated as the spatial average of DJF precipitation change for groups of $2.5^\circ \times 2.5^\circ$ grid boxes shown in Figure 3c. For each of these regions, the distribution of precipitation change is then calculated for (i) the original set of CMIP5 models, (ii) the $\sum_{i=1}^5 \binom{36}{i}$ subensembles, and (iii) the Pareto-optimal solutions of Figure 2d. Figure 3a shows box and

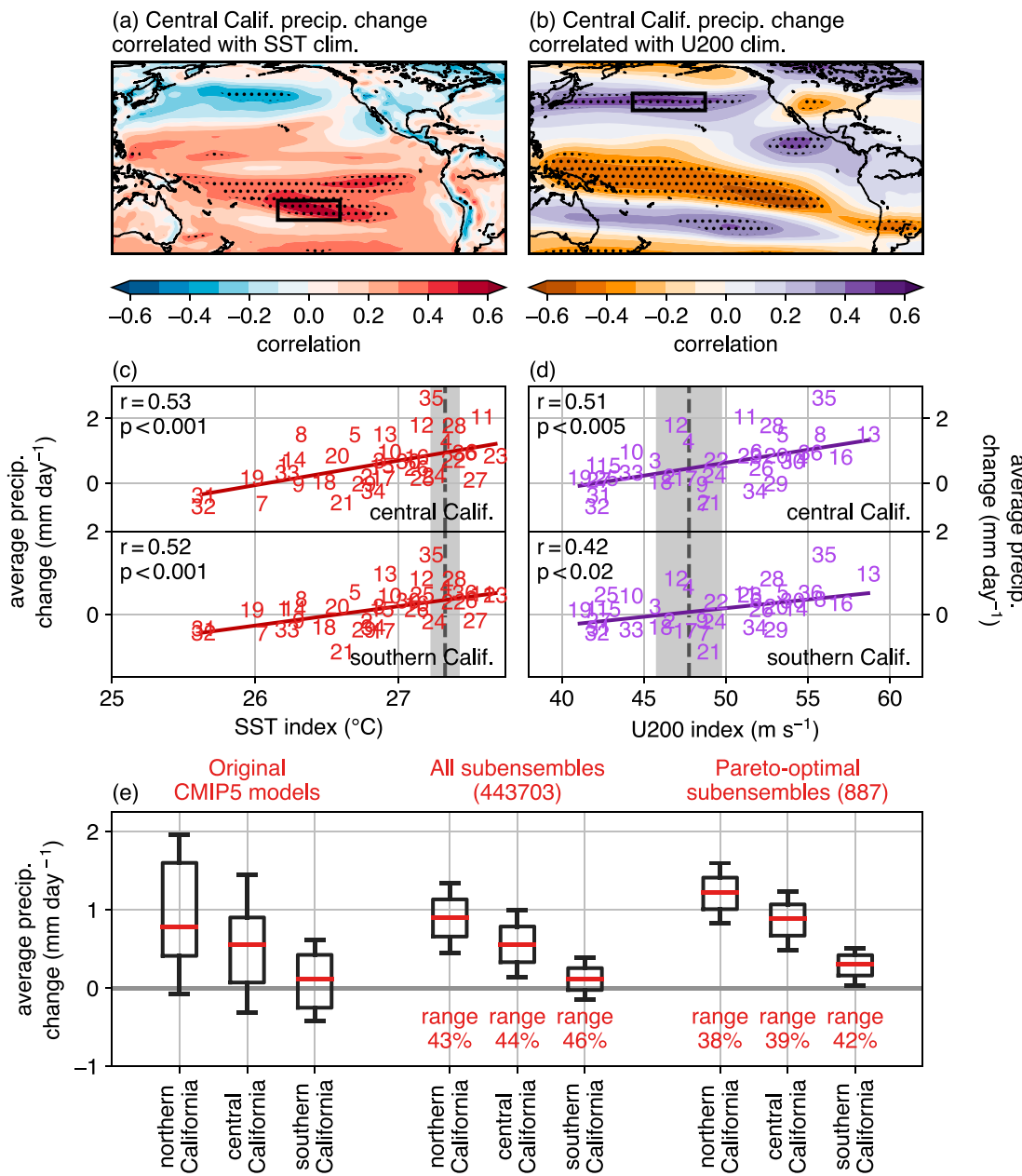


Figure 4. Grid point correlation maps between CMIP5 model climatologies in (a) SSTs or (b) 200 hPa zonal winds with central California precipitation changes (spatial mean of red grid boxes in Figure 3c). Black boxes correspond to latitude/longitude ranges of 25°S–15°S/210°E–240°E (Figure 4a) and 30°N–40°N/170°E–205°E (Figure 4b). (c and d) Regional averages in these boxes for each CMIP5 climatology represent the horizontal axes. Model numbers correspond to the legend of Figure 2, vertical axes show average precipitation anomalies over central/southern California grid boxes, and lines show least squares linear regressions across models (with the associated Pearson correlation and p value). Gray error bars show the 95% confidence interval of the observed internal variability. This was calculated as $\pm 1.96 \times SE$, where the quantity $SE = \sigma / \sqrt{y}$ is the standard error of the mean, σ is the interannual standard deviation of DJF spatially averaged SSTs during 1980–2010, and y is the number of years (here, 30). (e) Box and whisker plots analogous to Figure 3a but for the smaller SSTs and 200 hPa zonal wind domains.

whisker plots of these distributions, and one can see the reductions in model achieved by this process. The full set of subensembles exhibits a 10th–90th percentile range that is about 43–46% of the original CMIP ensemble, and this primary reduction in spread is expected, since averaging model patterns together tends to cancel errors (e.g., Annan & Hargreaves, 2011; Knutti et al., 2010; Pincus et al., 2008). The 891-member Pareto-optimal set within that group is narrower still at about 30–31%. Conclusions from raw CMIP5 output about modest mean precipitation increases are therefore reinforced, with the added utility that these models have been subject to physically relevant, multiobjective climatological mean constraints.

To put these distributions into context, maps representing the Pareto-optimal results for 10th, median, and 90th percentile precipitation change (using the central California index) are plotted in Figures 3b–3d. Central California is used because of its relevance to water resource considerations (Dettinger et al., 2015). These patterns indicate variations in the magnitude and north-south gradient of the precipitation increase, while precipitation decreases tend to be restricted to the southeastern portion of the domain.

4.2. Connections to the Emergent Constraint Literature

Using this methodology within a more explicit emergent constraint framework, Figures 4a and 4b show correlation maps between end-of-century precipitation changes in the central California region with SST and 200 hPa zonal wind climatologies, giving a sense of where intermodel spread in SSTs and the upper level jet mean state are correlated with central California precipitation change. Black boxes indicate proximal centers of action for these correlation values.

Following steps typical of the emergent constraint literature, Figures 4c and 4d plot SST and 200 hPa zonal wind climatologies in the boxed regions of Figures 4a and 4b against California precipitation change, showing statistically significant correlations that could be used to help narrow end-of-century changes in precipitation in these regions. The Pareto fronts are similar to those shown in Figure 2, although for these smaller domains, they are shifted closer to the origin (Figure S5). Figure 4e demonstrates the effect of using these constraints within the Pareto-optimal subensemble framework. The emergent constraint-based metrics project a slightly increased median precipitation change relative to Figure 3a, but they do not further reduce the range of projections, and the corresponding maps of precipitation change are largely unaffected (Figure S6). Furthermore, narrowing the metrics of interest to small spatial regions may risk being overly specific to the set of models at hand. Using larger domains encompassing these regions (as in Figures 1–3) allows one to bring a wider set of physically based constraints to bear on the ensemble constraint process.

5. Summary and Conclusions

This study showcases an application of multiobjective optimization to climate model subensembles. Multiobjective optimization has the potential to address trade-offs among climate model performance metrics or objective functions, but applying it to a small ensemble that sparsely covers the objective function space would encounter problems yielding robust results. The much larger set of subensembles generated from models subsets is able to span the objective function space more continuously and facilitates this approach. Model subensembles can be thought of as playing a role analogous to interpolations using a meta-model or emulator in a perturbed physics ensemble, where interpolations are taken in the parameter space of a climate model, but in this case, the underlying differences in climate model parameterizations or formulation do not need to be known. The interpolations are instead done in the spatial fields of the ensemble subsets. The set of points in the space of objective functions evaluated from these forms a sufficiently dense “cloud” to estimate a relatively smooth Pareto front.

We identify the set of Pareto-optimal subensembles for a variety of fields relevant to California precipitation, and this information is used to provide constraints on end-of-century change for this region. The results are consistent with prior conclusions that California will experience modest wet season precipitation increases, with the possibility of drying excluded by this analysis at the 10% level for central and Southern California. We note that the California-specific metrics chosen here are not exhaustive—other objective functions may be important for precipitation change and its uncertainty in this region. In addition, we underline that typical caveats for emergent constraint approaches apply here: results depend on the underlying model ensemble as well as on the physical relevance and strength of the constraints chosen.

Mean winter precipitation change is addressed here because it is considered relatively uncertain, but other factors are important for California water resources. Evaporation and evapotranspiration are projected to increase throughout the year with global warming (Seager et al., 2014; Williams et al., 2015). Warming will also affect Sierra Nevada snowpack (Berg & Hall, 2017; Sun et al., 2016), leading to earlier snowmelt and decreased warm season streamflow (Kapnick and Hall, 2010, 2012), with negative consequences for water resources. And perhaps most importantly, there is mounting evidence for increases in precipitation extremes at global scales (Diffenbaugh et al., 2017; Neelin et al., 2017) and within California in particular (Berg & Hall, 2015; Dettinger, 2011; Hayhoe et al., 2004), and these can have substantial impacts on water infrastructure not captured by our results.

The techniques used here complement the emergent constraint literature and generalize its approach to include multiple performance metrics. We believe the appeal of our methodology is its ability to employ physically based diagnostics that encompass large geographic features of the climate system, such as the tropical Pacific Ocean or the midlatitude Pacific storm track, rather than depend on smaller domains that run the risk of being overprescribed and sensitive to the ensemble at hand. In addition, this approach can directly consider objective functions like accuracy in simulating precipitation climatology, even if such metrics do not exhibit clear emergent constraint behavior. Leveraging correlations between historical bias and end-of-century change is an important aspect of constraining climate model projections, and doing this in a multiobjective context allows for a broader set of constraints to be applied at once.

Acknowledgments

We thank two anonymous reviewers for their comments and feedback on this manuscript. This work was supported in part by the United States National Science Foundation (NSF) grant AGS-1540518 and the United States National Oceanic and Atmospheric Administration (NOAA) grant NA14OAR4310274. We acknowledge the World Climate Research Programme and thank the climate modeling groups responsible for producing and making available their output. Original climate model and observational/reanalysis data sets can be downloaded, respectively, from the Earth System Grid Federation portal (<https://esgf-node.llnl.gov/projects/cmip5/>) and the NOAA Earth System Research Laboratory gridded data website (<https://www.esrl.noaa.gov/psd/data/gridded/>). Python scripts used for figures/analysis will be made available via the MultiObjective Optimization of SubEnsembles (MOOSE) repository at <https://dept.atmos.ucla.edu/csi/software>. The NCAR Command Language version 6.3.0 (<https://doi.org/10.5065/D6WD3XH5>) was used to interpolate all data sets to a common grid. Plots were generated using Matplotlib, and maps were created using the Basemap Toolkit.

References

- Abramowitz, G., & Bishop, C. (2015). Climate model dependence and the ensemble dependence transformation of CMIP projections. *Journal of Climate*, 28(6), 2332–2348.
- Adler, R. F., Huffman, G. J., Chang, A., Ferraro, R., Xie, P.-P., Janowiak, J., ... Nelkin, E. (2003). The version-2 Global Precipitation Climatology Project (GPCP) monthly precipitation analysis (1979–present). *Journal of Hydrometeorology*, 4, 1147–1167.
- Allen, R. J., & Luptowicz, R. (2017). El niño-like teleconnection increases California precipitation in response to warming. *Nature Communications*, 8, 16055.
- Annan, J., & Hargreaves, J. (2011). Understanding the CMIP3 multimodel ensemble. *Journal of Climate*, 24(16), 4529–4538.
- Berg, N., & Hall, A. (2015). Increased interannual precipitation extremes over California under climate change. *Journal of Climate*, 28(16), 6324–6334.
- Berg, N., & Hall, A. (2017). Anthropogenic warming impacts on California snowpack during drought. *Geophysical Research Letters*, 44, 2511–2518. <https://doi.org/10.1002/2016GL072104>
- Bishop, C. H., & Abramowitz, G. (2013). Climate model dependence and the replicate Earth paradigm. *Climate Dynamics*, 41(3–4), 885–900.
- Branke, J., Deb, K., & Slowinski, K. M. R. (Eds.) (2008). *Multiobjective Optimization: Interactive and Evolutionary Approaches* (470 p.). Berlin, Heidelberg: Springer.
- Brient, F., Schneider, T., Tan, Z., Bony, S., Qu, X., & Hall, A. (2016). Shallowness of tropical low clouds as a predictor of climate models' response to warming. *Climate Dynamics*, 47(1–2), 433–449.
- Ceppi, P., McCoy, D. T., & Hartmann, D. L. (2016). Observational evidence for a negative shortwave cloud feedback in middle to high latitudes. *Geophysical Research Letters*, 43, 1331–1339. <https://doi.org/10.1002/2015GL067499>
- Chang, E. K., Zheng, C., Lanigan, P., Yau, A. M., & Neelin, J. D. (2015). Significant modulation of variability and projected change in California winter precipitation by extratropical cyclone activity. *Geophysical Research Letters*, 42, 5983–5991. <https://doi.org/10.1002/2015GL064424>
- Chang, E. K. M., Guo, Y., & Xia, X. (2012). CMIP5 multimodel ensemble projection of storm track change under global warming. *Journal of Geophysical Research: Atmospheres*, 117, D23118. <https://doi.org/10.1029/2012JD018578>
- Choi, J., Lu, J., Son, S.-W., Frierson, D. M., & Yoon, J.-H. (2016). Uncertainty in future projections of the North Pacific subtropical high and its implication for California winter precipitation change. *Journal of Geophysical Research: Atmospheres*, 121, 795–806. <https://doi.org/10.1002/2015JD023858>
- Chou, C., & Neelin, J. D. (2004). Mechanisms of global warming impacts on regional tropical precipitation. *Journal of Climate*, 17(13), 2688–2701.
- Coello Coello, C., Lamont, G. B., & van Velhuizen, D. A. (2007). *Evolutionary Algorithms for Solving Multi-Objective Problems* (2nd ed.). Genetic and Evolutionary Computation. US: Springer.
- Collins, M., Knutti, R., Arblaster, J., Dufresne, J.-L., Fichefet, T., Friedlingstein, P., ... Wehner, M. (2013). Long-term climate change: projections, commitments and irreversibility. In T. F. Stocker, et al. (Eds.), *Climate Change 2013: The Physical Science Basis. Contribution of Working Group I to the Fifth Assessment Report of the Intergovernmental Panel on Climate Change*, *Climate Change 2013: The Physical Science Basis* (pp. 1029–1136). Cambridge, UK: Cambridge University Press.
- DeAngelis, A. M., Qu, X., Zelinka, M. D., & Hall, A. (2015). An observational radiative constraint on hydrologic cycle intensification. *Nature*, 528(7581), 249–253.
- Deb, K., Pratap, A., Agarwal, S., & Meyarivan, T. (2002). A fast and elitist multiobjective genetic algorithm: NSGA-II. *IEEE Transactions on Evolutionary Computation*, 6(2), 182–197.
- Dee, D. P., Uppala, S. M., Simmons, A. J., Berrisford, P., Poli, P., Kobayashi, S., ... Vitart, F. (2011). The ERA-interim reanalysis: Configuration and performance of the data assimilation system. *Quarterly Journal of the Royal Meteorological Society*, 137(656), 553–597.
- Delcambre, S. C., Lorenz, D. J., Vimont, D. J., & Martin, J. E. (2013a). Diagnosing Northern Hemisphere jet portrayal in 17 CMIP3 global climate models: Twentieth-century intermodel variability. *Journal of Climate*, 26(14), 4910–4929.
- Delcambre, S. C., Lorenz, D. J., Vimont, D. J., & Martin, J. E. (2013b). Diagnosing Northern Hemisphere jet portrayal in 17 CMIP3 global climate models: Twenty-first-century projections. *Journal of Climate*, 26(14), 4930–4946.
- Dettinger, M. (2011). Climate change, atmospheric rivers, and floods in California—A multimodel analysis of storm frequency and magnitude changes. *JAWRA Journal of the American Water Resources Association*, 47(3), 514–523.
- Dettinger, M., Udall, B., & Georgakakos, A. (2015). Western water and climate change. *Ecological Applications*, 25(8), 2069–2093.
- Diffenbaugh, N. S., Singh, D., Mankin, J. S., Horton, D. E., Swain, D. L., Touma, D., ... Rajaratnam, B. (2017). Quantifying the influence of global warming on unprecedented extreme climate events. *Proceedings of the National Academy of Sciences of the United States of America*, 114(19), 4881–4886.
- Fasullo, J. T., & Trenberth, K. E. (2012). A less cloudy future: The role of subtropical subsidence in climate sensitivity. *Science*, 338(6108), 792–794.
- Flato, G., Marotzke, J., Abiodun, B., Braconnot, P., Chou, S. C., Collins, W. J., ... Rummukainen, M. (2013). Evaluation of climate models. In T. F. Stocker, et al. (Eds.), *Climate Change 2013: The Physical Science Basis. Contribution of Working Group I to the Fifth Assessment Report of the Intergovernmental Panel on Climate Change*, *Climate Change 2013: The Physical Science Basis* (pp. 741–866). Cambridge, UK: Cambridge University Press.
- Gleckler, P. J., Taylor, K. E., & Doutriaux, C. (2008). Performance metrics for climate models. *Journal of Geophysical Research: Atmospheres*, 113, D06104. <https://doi.org/10.1029/2007JD008972>

- Gordon, N. D., & Klein, S. A. (2014). Low-cloud optical depth feedback in climate models. *Journal of Geophysical Research: Atmospheres*, 119, 6052–6065. <https://doi.org/10.1002/2013JD021052>
- Greve, P., Orlowsky, B., Mueller, B., Sheffeld, J., Reichstein, M., & Seneviratne, S. I. (2014). Global assessment of trends in wetting and drying over land. *Nature Geoscience*, 7, 716–721.
- Hall, A., & Qu, X. (2006). Using the current seasonal cycle to constrain snow albedo feedback in future climate change. *Geophysical Research Letters*, 33, L03502. <https://doi.org/10.1029/2005GL025127>
- Hayhoe, K., Cayan, D., Field, C. B., Frumhoff, P. C., Maurer, E. P., Miller, N. L., ... Verville, J. H. (2004). Emissions pathways, climate change, and impacts on California. *Proceedings of the National Academy of Sciences of the United States of America*, 101(34), 12,422–12,427.
- Held, I. M., & Soden, B. J. (2006). Robust responses of the hydrological cycle to global warming. *Journal of Climate*, 19(21), 5686–5699.
- Herger, N., Abramowitz, G., Knutti, R., Angélil, O., Lehmann, K., & Sanderson, B. M. (2017). Selecting a climate model subset to optimise key ensemble properties. *Earth System Dynamics Discussions*, <https://doi.org/10.5194/esd-2017-28>, in review.
- Kapnick, S., & Hall, A. (2010). Observed climate–snowpack relationships in California and their implications for the future. *Journal of Climate*, 23(13), 3446–3456.
- Kapnick, S., & Hall, A. (2012). Causes of recent changes in western North American snowpack. *Climate Dynamics*, 38(9–10), 1885–1899.
- Kay, J. E., Deser, C., Phillips, A., Mai, A., Hannay, C., Strand, G., ... Vertenstein, M. (2015). The Community Earth System Model (CESM) large ensemble project: A community resource for studying climate change in the presence of internal climate variability. *Bulletin of the American Meteorological Society*, 96(8), 1333–1349.
- Klein, S. A., & Hall, A. (2015). Emergent constraints for cloud feedbacks. *Current Climate Change Reports*, 1(4), 276–287.
- Klocke, D., Pincus, R., & Quasas, J. (2011). On constraining estimates of climate sensitivity with present-day observations through model weighting. *Journal of Climate*, 24, 6092–6099.
- Knutti, R. (2010). The end of model democracy? *Climatic Change*, 102, 395–404.
- Knutti, R., Masson, D., & Gettelman, A. (2013). Climate model genealogy: Generation CMIP5 and how we got there. *Geophysical Research Letters*, 40, 1194–1199. <https://doi.org/10.1002/grl.50256>
- Knutti, R., Furrer, R., Tebaldi, C., Cermak, J., & Meehl, G. A. (2010). Challenges in combining projections from multiple climate models. *Journal of Climate*, 23, 2739–2758.
- Knutti, R., Sedláček, J., Sanderson, B. M., Lorenz, R., Fischer, E. M., & Eyring, V. (2017). A climate model projection weighting scheme accounting for performance and interdependence. *Geophysical Research Letters*, 44, 1909–1918. <https://doi.org/10.1002/2016GL072012>
- Langenbrunner, B., & Neelin, J. D. (2017). Multiobjective constraints for climate model parameter choices: Pragmatic Pareto fronts in CESM1. *Journal of Advances in Modeling Earth Systems*, 9, 2008–2026. <https://doi.org/10.1002/2017MS000942>
- Langenbrunner, B., Neelin, J. D., Lintner, B. R., & Anderson, B. T. (2015). Patterns of precipitation change and climatological uncertainty among CMIP5 models, with a focus on the midlatitude Pacific storm track. *Journal of Climate*, 28, 7858–7872.
- Lu, J., Vecchi, G. A., & Reichler, T. (2007). Expansion of the Hadley cell under global warming. *Geophysical Research Letters*, 34, L06805. <https://doi.org/10.1029/2006GL028443>
- Marler, R. T., & Arora, J. S. (2004). Survey of multi-objective optimization methods for engineering. *Structural and Multidisciplinary Optimization*, 26, 369–395.
- Masson, D., & Knutti, R. (2011). Climate model genealogy. *Geophysical Research Letters*, 38, L08703. <https://doi.org/10.1029/2011GL046864>
- Myers, T. A., & Norris, J. R. (2016). Reducing the uncertainty in subtropical cloud feedback. *Geophysical Research Letters*, 43, 2144–2148. <https://doi.org/10.1002/2015GL067416>
- Neelin, J., Langenbrunner, B., Meyerson, J., Hall, A., & Berg, N. (2013). California winter precipitation change under global warming in the Coupled Model Intercomparison Project phase 5 ensemble. *Journal of Climate*, 26(17), 6238–6256.
- Neelin, J. D., Sahany, S., Stechmann, S. N., & Bernstein, D. N. (2017). Global warming precipitation accumulation increases above the current-climate cutoff scale. *Proceedings of the National Academy of Sciences of the United States of America*, 114(6), 1258–1263.
- Neelin, J. D., Bracco, A., Luo, H., McWilliams, J. C., & Meyerson, J. E. (2010). Considerations for parameter optimization and sensitivity in climate models. *Proceedings of the National Academy of Sciences of the United States of America*, 107(50), 21,349–21,354.
- Pareto, V. (1906). *Manuale di economia politica* (Vol. 13). Milano: Società Editrice.
- Pierce, D. W., Barnett, T. P., Santer, B. D., & Gleckler, P. J. (2009). Selecting global climate models for regional climate change studies. *Proceedings of the National Academy of Sciences of the United States of America*, 106(21), 8441–8446.
- Pierce, D. W., Das, T., Cayan, D. R., Maurer, E. P., Miller, N. L., Bao, Y., ... Tyree, M. (2013). Probabilistic estimates of future changes in California temperature and precipitation using statistical and dynamical downscaling. *Climate Dynamics*, 40(3–4), 839–856.
- Pincus, R., Batstone, C. P., Hofmann, R. J. P., Taylor, K. E., & Gleckler, P. J. (2008). Evaluating the present-day simulation of clouds, precipitation, and radiation in climate models. *Journal of Geophysical Research*, 113, D14209. <https://doi.org/10.1029/2007JD009334>
- Qu, X., Hall, A., Klein, S. A., & DeAngelis, A. M. (2015). Positive tropical marine low-cloud cover feedback inferred from cloud-controlling factors. *Geophysical Research Letters*, 42, 7767–7775. <https://doi.org/10.1002/2015GL065627>
- Reichler, T., & Kim, J. (2008). How well do coupled models simulate today's climate? *Bulletin of the American Meteorological Society*, 89(3), 303–311.
- Rienecker, M. M., Suarez, M. J., Gelaro, R., Todling, R., Bacmeister, J., Liu, E., ... Woollen, J. (2011). MERRA: NASA's modern-era retrospective analysis for research and applications. *Journal of Climate*, 24(14), 3624–3648.
- Roderick, M. L., Sun, F., Lim, W. H., & Farquhar, G. D. (2014). A general framework for understanding the response of the water cycle to global warming over land and ocean. *Hydrology and Earth System Sciences*, 18(5), 1575–1589.
- Sanderson, B. M., & Knutti, R. (2012). On the interpretation of constrained climate model ensembles. *Geophysical Research Letters*, 39, L16708. <https://doi.org/10.1029/2012GL052665>
- Sanderson, B. M., Wehner, M., & Knutti, R. (2017). Skill and independence weighting for multi-model assessments. *Geoscientific Model Development*, 10(6), 2379–2395.
- Santer, B., Taylor, K., Gleckler, P., Bonfils, C., Barnett, T., Pierce, D., ... Wehner, M. F. (2009). Incorporating model quality information in climate change detection and attribution studies. *Proceedings of the National Academy of Sciences of the United States of America*, 106(35), 14,778–14,783.
- Scheff, J., & Frierson, D. M. W. (2012a). Twenty-first-century multimodel subtropical precipitation declines are mostly midlatitude shifts. *Journal of Climate*, 25, 4330–4347.
- Scheff, J., & Frierson, D. M. W. (2012b). Robust future precipitation declines in CMIP5 largely reflect the poleward expansion of model subtropical dry zones. *Geophysical Research Letters*, 39, L18704. <https://doi.org/10.1029/2012GL052910>
- Seager, R., Neelin, D., Simpson, I., Liu, H., Henderson, N., Shaw, T., ... Cook, B. (2014). Dynamical and thermodynamical causes of large-scale changes in the hydrological cycle over North America in response to global warming. *Journal of Climate*, 27(20), 7921–7948. <https://doi.org/10.1175/JCLI-D-14-00153.1>

- Sherwood, S. C., Bony, S., & Dufresne, J.-L. (2014). Spread in model climate sensitivity traced to atmospheric convective mixing. *Nature*, 505(7481), 37–42.
- Simpson, I. R., Seager, R., & Ting, T. A. (2016). Mingfang ad Shaw. *Nature Climate Change*, 6, 65–70.
- Stocker, T. F., Qin, D., Plattner, G.-K., Tignor, M., Allen, S. K., Boschung, J., ... Midgley, P. M. (2013). *Climate Change 2013: The Physical Science Basis. Contribution of Working Group I to the Fifth Assessment Report of the Intergovernmental Panel on Climate Change* (Vol. 5, pp. 1535). Cambridge, UK: Cambridge University Press.
- Su, H., Jiang, J. H., Zhai, C., Shen, T. J., Neelin, J. D., Stephens, G. L., & Yung, Y. L. (2014). Weakening and strengthening structures in the Hadley circulation change under global warming and implications for cloud response and climate sensitivity. *Journal of Geophysical Research: Atmospheres*, 119, 5787–5805. <https://doi.org/10.1002/2014JD021642>
- Su, H., Jiang, J. H., Neelin, J. D., Shen, T. J., Zhai, C., Yue, Q., ... Yung, Y. L. (2017). Tightening of tropical ascent and high clouds key to precipitation change in a warmer climate. *Nature Communications*, 8, 15771. <https://doi.org/10.1038/ncomms15771>
- Sun, F., Hall, A., Schwartz, M., Walton, D. B., & Berg, N. (2016). Twenty-first-century snowfall and snowpack changes over the Southern California mountains. *Journal of Climate*, 29(1), 91–110.
- Taylor, K. E., Stouffer, R. J., & Meehl, G. A. (2012). An overview of CMIP5 and the experiment design. *Bulletin of the American Meteorological Society*, 93(4), 485–498.
- Tebaldi, C., & Knutti, R. (2007). The use of the multi-model ensemble in probabilistic climate projections. *Philosophical Transactions of the Royal Society A: Mathematical, Physical and Engineering Sciences*, 365(1857), 2053–2075.
- Tebaldi, C., & Sansó, B. (2009). Joint projections of temperature and precipitation change from multiple climate models: A hierarchical Bayesian approach. *Journal of the Royal Statistical Society: Series A (Statistics in Society)*, 172(1), 83–106.
- Tian, B. (2015). Spread of model climate sensitivity linked to double-intertropical convergence zone bias. *Geophysical Research Letters*, 42, 4133–4141. <https://doi.org/10.1002/2015GL064119>
- Trenberth, K. E. (2011). Changes in precipitation with climate change. *Climate Research*, 47(1-2), 123–138.
- Trenberth, K. E., & Fasullo, J. T. (2010). Simulation of present-day and twenty-first-century energy budgets of the southern oceans. *Journal of Climate*, 23(2), 440–454.
- Tsushima, Y., Ringer, M. A., Koshiro, T., Kawai, H., Roehrig, R., Cole, J., ... Webb, M. J. (2016). Robustness, uncertainties, and emergent constraints in the radiative responses of stratocumulus cloud regimes to future warming. *Climate dynamics*, 46(9-10), 3025–3039.
- Volodin, E. (2008). Relation between temperature sensitivity to doubled carbon dioxide and the distribution of clouds in current climate models. *Izvestiya Atmospheric and Oceanic Physics*, 44(3), 288–299.
- Williams, A. P., Seager, R., Abatzoglou, J. T., Cook, B. I., Smerdon, J. E., & Cook, E. R. (2015). Contribution of anthropogenic warming to California drought during 2012–2014. *Geophysical Research Letters*, 42, 6819–6828. <https://doi.org/10.7916/D8FB52C5>
- Woodruff, M. J., & Herman, J. D. (2014). Pareto.py: Nondominated sorting for multi-objective problems. Retrieved from <https://github.com/matthewjwoodruff/pareto.py>. Accessed August 2016
- Zhai, C., Jiang, J. H., & Su, H. (2015). Long-term cloud change imprinted in seasonal cloud variation: More evidence of high climate sensitivity. *Geophysical Research Letters*, 42, 8729–8737. <https://doi.org/10.1002/2015GL065911>